Planning Under Non-Rational Perception of Uncertain Spatial Costs

Aamodh Suresh and Sonia Martínez

***Abstract*—This work investigates the design of risk-perception-aware motion-planning strategies that incorporate non-rational risk associated with uncertain spatial costs. Our proposed method employs the Cumulative Prospect Theory (CPT) to generate a perceived risk map over a given environment. CPT-like perceived risks and path-length metrics are then combined to define a cost function that is compliant with the requirements of asymptotic optimality of sampling-based motion planners (RRT*). The modeling power of CPT is illustrated in theory and in simulation, along with a comparison to other risk perception models like Conditional Value at Risk (CVaR). Theoretically, we define a notion of expressiveness for a risk perception model and show that CPT's is higher than that of CVaR and expected risk. We then show that this expressiveness translates to our path planning setting, where we observe that a planner equipped with CPT together with a simultaneous perturbation stochastic approximation (SPSA) method can better approximate arbitrary paths in an environment. Additionally, we show in simulation that our planner captures a rich set of meaningful paths, representative of different risk perceptions in a custom environment. We then compare the performance of our planner with T-RRT* (a planner for continuous cost spaces) and Risk-RRT* (a risk-aware planner for dynamic human obstacles) through simulations in cluttered and dynamic environments respectively, showing the advantage of our proposed planner.**

***Index Terms*—Behavior-based systems, human-aware motion planning, human-centered robotics, motion and path planning.**

I. Introduction

MOTIVATION: Autonomous robots from industrial manipulators to robotic swarms [1]–[3], are less isolated and increasingly more interactive. Arguably, most environments where these robots operate, have an associated spatial cost, which can lead to a robot's loss or damage. In more complex scenarios, a decision maker (DM) may be directly involved with the motion of an autonomous system, such as in robotic surgery, search and rescue operations, or autonomous car driving. The risk perceived from these costs or losses could vary among different DMs. This motivates the consideration of richer models that are inclusive of non-rational perception of spatial costs in motion planning. With this goal, we aim to study how Cumulative Prospect Theory (CPT) [4] can be included into path planning, and compare its paths with those obtained from other risk perception models. Fig. 1 shows a preview of how a non-rational DM's perception of the same environment influences the path produced to reach a goal.

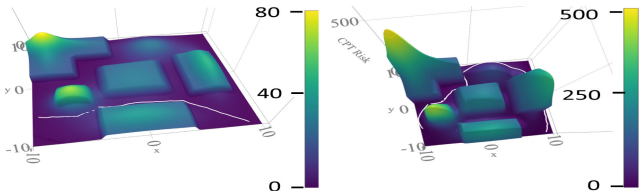

(a) Motion plan with expected risk (b) Motion plan with CPT risks

Fig. 1. Environment perception and sampling-based motion planning (chosen path in white) in risky environments using a) Rational perception using expected risk, b) DM's Risk-Averse perception. (a) Motion plan with expected risk. (b) Motion plan with CPT risks.

Related Work: Traditional risk-aware path planning considers risk in the form of motion and state uncertainty [5], collision time [6], or sensing uncertainty [7]. Chance constrained approaches [8], [9] are used to handle agent and environment uncertainty in a robust manner, however discrete polyhedral obstacles are considered which cannot incorporate continuous spatial costs. Stochastic dynamic programming [10] in used in dynamic environments to locally integrate planning and estimation without optimality guarantees. Moreover, in all the above works, how the risks and uncertainties are perceived or relatively weighted has been overlooked. A few recent works [11] contemplate risk perception models, but assume rational DMs using coherent risk measures like Conditional Value at Risk (CVaR) [12]. These measures use axioms that assume rationality and linearity of the DM's risk perception [13]. However, research in Psychophysics [14] and behavioral economics [4] advocate a fundamental non-linear perception (with surprisingly similar power laws) among DMs. The latter uses additional non-linear uncertainty perception to explain the observed non-rational decision making. CPT has been extensively used in engineering applications like traffic routing [15], network protection [16], stochastic optimization [17], and safe shipping [18] to model non-rational decision making. However, CPT is yet to be applied in motion planning.

Regarding planning algorithms, RRT* [19] has been the basis for many motion planners due to its asymptotic optimality properties (guaranteeing consistency) and ability to solve complex problems [20]. Risk (Risk-RRT* [21]) and uncertainty [22] have been an ingredient of planning problems involving a human, but have been mainly modeled in a probabilistic manner [23]

Manuscript received October 8, 2020; accepted February 25, 2021. Date of publication March 18, 2021; date of current version April 8, 2021. This letter was recommended for publication by Associate Editor N. Amato and M. Morales upon evaluation of the reviewers' comments. This work was supported by ONR under Grant ONR - N00014-19-1-2471. *(Corresponding author: Aamodh Suresh.)*

The authors are with the Department of Mechanical and Aerospace Engineering, University of California at San Diego, La Jolla, CA 92093 USA (e-mail: aasuresh@eng.ucsd.edu; soniamd@ucsd.edu).

This letter has supplementary downloadable material available at https://doi.org/10.1109/LRA.2021.3067272, provided by the authors.

Digital Object Identifier 10.1109/LRA.2021.3067272

with discrete obstacles. Although Risk-RRT* considers risk and asymptotic optimality, it doesn't incorporate uncertainty or different risk-perception models. In addition, very few RRT* planning frameworks model environments as continuous cost maps (with the exception of T-RRT* [24] and [25]). However, these works do not explicitly handle cost uncertainty or risk. In addition, their transition-test mechanism does not always produce desirable paths quickly (see Section VII).

Contributions: Firstly, we adapt CPT into path planning to model non-rational perception of spatial cost, capturing a larger variety of risk perception, and extending the existing literature. Secondly, we generate consistent (asymptotically optimal) and desirable (risk perception aware) paths using a sampling-based (RRT*-based) planning algorithm on the perceived risky environment. We then compare our planner's performance with T-RRT* (continuous cost space planner) and Risk-RRT* (risk-aware planner) through simulations and show that our proposed planner can generate better paths in comparison. Finally, we define the notion of "expressiveness" for a risk perception model and theoretically show that CPT's is higher than that of CVaR and expected risk. In simulations, using SPSA, we illustrate the above hierarchy by observing that our CPT-based planner can better approximate arbitrary paths in an environment. We note here that we merely examine CPT-based perception models for motion planning and leave the validation of these models for future work.

II. Preliminaries

Here we describe some basic notations[1] used along with a concise description of CPT (refer to [26] for more details).

CPT is a non-rational decision making model which incorporates non-linear perception of uncertain costs. Let us suppose a DM is presented with a set of prospects $\{\rho^1, \ldots, \rho^k, \ldots, \rho^K\}$, representing potential outcomes and their probabilities, $\rho^k = \{(\rho_i^k, p_i^k)\}_{i=1}^M$. That is, there are M possible outcomes associated with a prospect k, given by $\rho_i^k \in \mathbb{R}_{\geq 0}$, which occurs with a probability p_i^k.

The outcomes are arranged in a decreasing order $\rho_M^k < \rho_{M-1}^k < \ldots < \rho_1^k$ and $\sum_{i=1}^M p_i^k = 1$. The outcomes of prospect k describe the random cost,[2] of choosing prospect k.

We define a utility function, $v : \mathbb{R}_{\geq 0} \to \mathbb{R}_{\geq 0}$ modeling a DM's perceived cost and $w : [0, 1] \to [0, 1]$ as the probability weighting function which represents the DM's perceived uncertainty. The CPT utility function v takes the form:

$$v(\rho) = \lambda \cdot \rho^{\gamma}, \tag{1}$$

where $0 < \gamma < 1$ and $\lambda > 1$. Nominal parameters $\gamma = 0.88$ and $\lambda = 2.25$ are suggested in [4] for monetary lottery scenarios, however this may not hold for our application scenario. The parameter λ represents "cost aversion" with greater values implying stronger aversion indicative of higher perceived costs, as shown in Fig. 2(a). The parameter γ represents "cost sensitivity" with lower values implying greater indifference towards cost ρ, which is indicated in Fig. 2(b).

We will use the popular Prelec's probability weighting function [26], [27] indicative of perceived uncertainty:

$$w(p) = e^{-\beta(-\log p)^{\alpha}}, \alpha > 0, \beta > 0, w(0) = 0. \tag{2}$$

Fig. 2(c) and 2(d) show changes in uncertainty perception from varying α and β respectively. With low α and β values, one can get "uncertainty averse" behavior, with $w(p) > p$ implying more certainty in unlikely outcomes, as seen in Figures 2(c) and 2(d). With high α and β values, we get "uncertainty insensitive" behavior (when $w(p) < p$),implying that the DM only considers more certain outcomes.

A DM under consideration can be categorized by the parameters $\Theta = \{\alpha, \beta, \gamma, \lambda\}$. Using the non-linear perception functions v and w, CPT calculates a value function $R^c(\rho)$, indicating the perceived risk value of the prospect ρ. This calculation is detailed in Section IV for our context.

III. Environment Setup and Problem Statement

Here, we consider spatial sources of risk embedded in the $\mathscr{C}$ space. Our starting point is an uncertain cost $\rho(x)$ that aims to quantify objectively the (negative) consequences of being at a location x. In this work, we will assume that the cost at a location $x \in \mathscr{C}$ has been characterized as a random variable $\rho(x)$ with a mean $\rho_\mu(x) \in \mathbb{R}_{\geq 0}$ and standard deviation $\rho_\sigma(x) \in \mathbb{R}_{\geq 0}$, for each $x \in \mathscr{C}$.

For more context, we provide two examples explaining the cost sources for scenarios involving environmental hazards and moving obstacles; see [28] for more information. First, consider an emergency drone equipped with a thermal scanner, navigating in a building which is ablaze. Here, the cost function can be proportional to the spatial temperature profile. Noisy sensors result in an uncertain spatial cost value $\rho(x)$ with moments $\rho_\mu(x)$ and $\rho_\sigma(x)$ derived from the sensor's uncertainty. In another case, suppose a robot is at $x \in \mathscr{C}$ and obstacle at $y \in \mathscr{C}$. Then, we can define a spatial cost as the possible damage to the robot [3] which is inversely proportional to the distance between x and y. That is, $\rho(x) \propto \|y - x\|^{-1}$. Since the future actions of the obstacle are unknown and/or the obstacle is localized imprecisely, $\rho(x)$ is uncertain with moments corresponding to possibly both sensing and action uncertainty of the obstacle. Above examples are also explored in simulations in Section VII.

Our notions of "risk" and "risk perception" relate to the way in which the values of $\rho(x)$ are scaled and averaged in expectation. That is, risk is a moment of a given uncertain cost $\rho(x)$. In this work, we use non-rational perception of $\rho(x)$ via CPT to plan paths by solving:

Problem 1: *(CPT environment generator). Given the configuration space $\mathscr{C}$ containing the uncertain cost ρ along with the DM's CPT parameters Θ, obtain a DM's (non-rational) perceived risk R^c consistent with CPT theory.*

Problem 2: *(Planning with perceived risk). Given a start and goal points x_s and x_g, compute a desirable path P from x_s to x_g in accordance with the DM's perceived risk R^c.*

[1] We let $\mathbb{R}$ denote real numbers, $\mathbb{Z}_{\geq 0}$ denote the positive integers, and $\mathbb{R}_{\geq 0}$ the space of non negative real numbers. Also, $\mathbb{R}^n$ and $\mathscr{C} \subset \mathbb{R}^n$ denote the n-dimensional real vector space and the configuration space used for planning. We use $\|.\|$ for the Euclidean norm and $\circ$ for the composition of two functions, that is $f(g(x)) = f \circ g(x)$. We model a tree by an directed graph $G = (V, E)$, where $V = \{1, \ldots, T\}$ denotes the set of sampled points (vertices of the graph), and $E \subset V \times V$, denotes the set of edges of the graph.

[2] CPT has an alternate perception model for random rewards [26] which is not used here since we are interested in cost perception.

[3] or psychological discomfort for a human, who is treated as an obstacle.

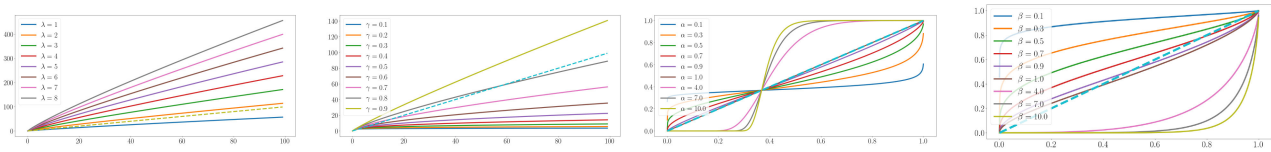

(a) Change in risk aversion λ with $\gamma = 0.88$ (b) Change in risk sensitivity γ with $\lambda = 2.25$ (c) Change in α with $\beta = 1$ (d) Change in β with $\alpha = 0.74$

Fig. 2. Variation of risk aversion, risk sensitivity and uncertainty perception using CPT. (a)-(b) show risk perception with x-axis indicating the associated risk, ρ, and the y-axis showing the perceived risk, v. The dotted line indicates the line $v = \rho$. (c)-(d) show uncertainty perception with x-axis indicating probabilities p and y-axis showing their perception w, with the dotted line depicting $w = p$.

Algorithm 1: CPT Environment (CPT-Env).

Input: $\rho_\mu(x)$, $\rho_\sigma(x)$, Θ, $\{p_1, ..., p_M\}$; Output : $R^c(x)$
for $i \in \{1, ..., M\}$ **do**
  $y_i(x), y_{i+1}(x) \leftarrow discretize(p_i(x), p_{i+1}(x))$;
  $\rho_i(x) \leftarrow \frac{y_{i+1}(x) - y_i(x)}{2}$;
end
$w \circ p(x) \leftarrow e^{-\beta(-\log \circ p(x))^\alpha}$; $v \circ \rho(x) \leftarrow \lambda(\rho(x))^\gamma$;
for $j \in \{1, ..., M\}$ **do**
  $\pi_j \leftarrow w \circ S_j(p_1, \ldots, p_M) - w \circ S_{j+1}(p_1, \ldots, p_M)$;
end
$R^c(x) \leftarrow \sum_{j=1}^{M} (v \circ \rho_j(x))(\pi_j \circ p(x))$;

Problem 3: *(CPT planner evaluation). Given a $\mathscr{C}$, and an uncertain cost ρ along with a drawn path P_d, evaluate the CPT planner as a model approximator to generate the perceived risk R^c representing the drawn path P_d.*

Now we solve these in Sections IV, V and VI respectively.

IV. Risk Perception using CPT

We start by addressing Problem 1. Consider that an uncertain cost $\rho(x)$ is given, for all $x \in \mathscr{C}$, which we approximate via its first two moments, a mean value $\rho_\mu(x) \in \mathbb{R}_{\geq 0}$ and a standard deviation $\rho_\sigma(x) \in \mathbb{R}_{\geq 0}$. In what follows, we discretize[4] $\rho(x)$ by considering $M \in \mathbb{Z}_{\geq 0}$ bins, and a set of possible cost values $\rho(x) \triangleq \{\rho_1(x), \ldots, \rho_M(x)\}$, with $\rho_M(x) < \rho_{M-1}(x) < \cdots < \rho_1(x)$ and their corresponding probabilities $p(x) \triangleq \{p_1(x), \ldots, p_M(x)\}$, such that $\sum_{i=1}^{M} p_i(x) = 1 \ \forall x \in \mathscr{C}$. Further, we assume that $p_i(x_1) = p_i(x_2) \equiv p_i, \ \forall x_1, x_2 \in \mathscr{C}$ and $i \in \{1, \ldots, M\}$. Note that we can do this wlog by discretizing the continuous RV appropriately, see Algorithm 1. The function $discretize$ finds $y_i(x) < y_{i+1}(x)$ such that $\mathbb{P}[y_i(x) \leq \rho(x) \leq y_{i+1}(x)] = p_{i+1}(x) - p_i(x)$.

Now, the expected Risk $R^e(x)$ at a point x is

$$R^e(x) \triangleq \sum_{i=1}^{M} \rho_i(x) p_i(x). \tag{3}$$

That is, the expected risk $R^e : \mathscr{C} \to \mathbb{R}_{\geq 0}$ from (3), corresponds to a standard or rational notion of risk. From CPT [4], there is a notion of cumulative decision-weight functions $\Pi := \{\pi_1, \ldots, \pi_M\}$ used to non-rationally modify the perception of probabilities $p_i(x)$ in a cumulative fashion. Consider $S_j(p_1, \ldots, p_M) \triangleq \sum_{i=j}^{M} p_j$ and define

$$\pi_j = w \circ S_j(p_1, \ldots, p_M) - w \circ S_{j+1}(p_1, \ldots, p_M), \tag{4}$$

where we employ the weighting function w from (2).

With this, a DM's CPT risk $R^c : \mathscr{C} \to \mathbb{R}_{\geq 0}$ associated to the configuration space is given by:

$$R^c(x) \triangleq \sum_{j=1}^{M} (v \circ \rho_j(x))(\pi_j \circ p(x)). \tag{5}$$

We note that R^e and R^c are differentiable, which is important for the good behavior of the planner and used for the analysis in Section V. Pictorially, given an uncertain spatial cost ρ with the first moment ρ_μ (Fig. 3(b)) and second moment ρ_σ (Fig. 3(c)) across an environment, the DM's risk perception can vary from being rational (i.e. using expected risk R^e) to non-rational (i.e using CPT risk R^c). By varying Θ, CPT risk R^c can be tuned to represent risk averse and risk indifferent (Fig. 3(d)) perception, as well as uncertainty indifferent (Fig. 3(e)) to uncertainty averse (Fig. 3(f)) perception. Calculating the CPT perceived risk at x is summarized in Algorithm 1. We note that Algorithm 1 does not depend on the dimensionality of the $\mathscr{C}$ space, but on the discretization factor M. This environment representation is used for planning next.

V. Sampling-Based Planning Using Perceived Risk

Here, we use the CPT notions to derive new cost functions, which are used for planning in the DM's perceived environment generated in Section IV. In traditional RRT*, optimal planning is achieved using path length as a metric. In our setting, just path length is insufficient as it does not capture risk in the configuration space. Thus, we define cost functions that a) take into account perceived risk and path length of a path, and b) satisfy the requirements that guarantee the asymptotic performance of an RRT*-based planner.

Path costs functions Let two points $x, y \in \mathscr{C}$ be arbitrarily close. A decrease in risk is a desirable trait, hence it is reasonable to add an additional term in the cost only if $R(y) - R(x) \geq 0$, indicating an increase in the DM's perceived risk by traveling from x to y. Consider the set of paths $\mathscr{P}(\mathscr{C}) \triangleq \{\eta : [0, 1] \to \mathscr{C} \mid \eta(0) = x, \eta(1) = y\}$. First, we first define the cost $J^c : \mathscr{P}(\mathscr{C}) \to \mathbb{R}_{\geq 0}$ of a path $\eta \in \mathscr{P}(\mathscr{C})$. Let $\{0, t_1, t_2, \ldots, t_L = 1\}$ be a discretization of [0, 1], with $t_{\ell+1} - t_\ell = \Delta t$, for all ℓ. Then, a discrete approximation of the cost over η should be:

$$J^c(\eta) \approx \Delta t \sum_{\ell=1}^{L} \max\left\{0, \frac{R^c(\eta(t_{\ell+1})) - R^c(\eta(t_\ell))}{\Delta t}\right\} + \delta L(\eta),$$

[4]The discretization of the random cost function is used to be able to use CPT directly with discrete random variables. However, it is possible to generalize what follows to the continuous random variable case.

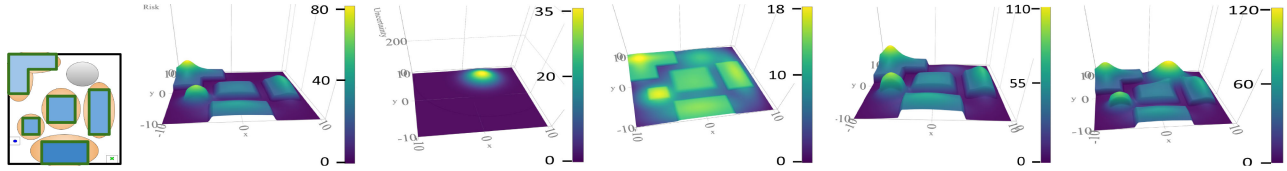

(a) Sketch of environment. (b) Mean cost ρ_μ (c) Uncertainty ρ_σ (d) Risk indifferent profile with $\Theta = \{0.74, 1, 0.3, 2.25\}$ (e) Uncertainty indifferent ($\Theta = \{0.74, 3, 0.88, 2.25\}$) (f) Uncertainty averse profile $\Theta = \{0.74, 0.05, 0.88, 2.25\}$

Fig. 3. Variety of risk perception using CPT of a given uncertain environment (a). X and Y axis of (b)-(f) denote the 2D environment of (a). The Z axis indicates the level of cost in (b), uncertainty in (c) and risk in (d)-(f).

Algorithm 2: CPT-RRT*.

Input: T, x_s, x_g ; Output : $G(V,E), P$
$V \leftarrow x_s$, $E \leftarrow \phi$, $J^c_{\text{cum}}(x_s) \leftarrow 0$;
for $i \in \{1, \ldots, T\}$ **do**
  $G \leftarrow (V,E)$; $x_{\text{rand}} \leftarrow Sample()$;
  $x_{\text{nrst}} \leftarrow Nearest(G, x_{\text{rand}})$; $x_{\text{new}} \leftarrow Steer(x_{\text{nrst}}, x_{\text{rand}})$;
  $V \leftarrow V \cup x_{\text{new}}$; $x_{\text{min}} \leftarrow x_{\text{nrst}}$;
  $X_{\text{near}} \leftarrow Near(G, x_{\text{new}}, \gamma_{\text{RRT}^*}, d)$;
  $c_{\text{min}} \leftarrow J^c_{\text{cum}}(x_{\text{nrst}}) + J^c(x_{\text{nrst}}, x_{\text{new}})$;
  for $x_{\text{near}} \in X_{\text{near}}$ **do**
    $c' \leftarrow J^c_{\text{cum}}(x_{\text{near}}) + J^c(x_{\text{near}}, x_{\text{new}})$;
    if $c' < c_{min}$ **then**
      $x_{\text{min}} \leftarrow x_{\text{near}}$; $c_{\text{min}} \leftarrow c'$;
    end
  end
  $J^c_{\text{cum}}(x_{\text{new}}) \leftarrow c_{\text{min}}$; $E \leftarrow E \bigcup (\{x_{\text{near}}, x_{\text{new}}\})$;
  for $x_{\text{near}} \in X_{\text{near}}$ **do**
    $c' \leftarrow J^c_{\text{cum}}(x_{\text{new}}) + J^c(x_{\text{new}}, x_{\text{near}})$;
    if $c' < J^c_{\text{cum}}(x_{\text{near}})$ **then**
      $x_{\text{par}} \leftarrow Parent(x_{\text{near}}, G)$;
      $E \leftarrow (E \setminus (\{x_{\text{par}}, x_{\text{near}}\})) \bigcup (\{x_{\text{new}}, x_{\text{near}}\})$;
      $X_{\text{chld}} \leftarrow Children(x_{\text{near}}, G)$;
      for $x_{\text{chld}} \in X_{\text{chld}}$ **do**
        $J^c_{\text{cum}}(x_{\text{chld}}) \leftarrow J^c_{\text{cum}}(x_{\text{chld}}) - J^c_{\text{cum}}(x_{\text{near}}) + c'$
      end
      $J^c_{\text{cum}}(x_{\text{near}}) \leftarrow c'$
    end
  end
end
$P \leftarrow Path(G, x_s, x_g)$;

where $L(\eta)$ denotes the arc-length of the curve η, and $\delta \in \mathbb{R}_{\geq 0}$ is a constant encoding an urgency versus risk tradeoff. The greater the δ value, the greater is the urgency and hence path length is more heavily weighted whereas, smaller δ indicates greater prominence towards risk. The appropriate choice of δ is discussed in Section VII. The above equation can be expressed as (see [28] for more details):

$$J^c(\eta) = \int_0^1 \max\{0, (R^c)'(\eta(t)) \cdot \eta'(t)\} \mathrm{d}t + \delta L(\eta). \quad (6)$$

From here, the cost of traveling from x to y is given by

$$J^c(x,y) \triangleq \min_{\eta \in \mathscr{P}(\mathscr{C}): \eta(0)=x, \eta(1)=y} J^c(\eta).$$

Similarly, the path cost using expected risk $J^e : \mathscr{P}(\mathscr{C}) \to \mathbb{R}_{\geq 0}$ can be obtained by replacing the CPT cost R^c in (6) with the expected risk R^e as calculated in (3).

Proposed Algorithm: Now RRT* can be adapted to our problem setting. Given $\mathscr{C}$, a number of iterations T and a start point $x_s \in \mathscr{C}$, we wish to produce graph $G(V,E)$, which represents a tree rooted at x_s whose nodes V are sample points in $\mathscr{C}$ and the edges E represent the path between the nodes in V. Let $J^c_{\text{cum}} : \mathscr{C} \to \mathbb{R}_{\geq 0}$ represent the cumulative cost to reach a point x from the root x_s of the tree $G(V,E)$ using the CPT cost metric (6). Similarly, we define $J^e_{\text{cum}} : \mathscr{C} \to \mathbb{R}_{\geq 0}$ for the expected cost function J^e. The other basic functional components of our algorithm CPT-RRT* (Algorithm 2) are similar to RRT* and are listed in the extended version [28]. We note that in order to compute J^c for each path, we approximate the cost as the sum of costs over its edges, (x_1, x_2), and for each edge we compute the cost as the differences $\max\{0, R^c(x_2) - R^c(x_1)\} + \delta L(x_1, x_2)$, where the latter is just the length of the edge. Then, this approximation will approach the computation of the real cost in the limit as the number of samples goes to infinity. The values R^c are evaluated according to Algorithm 1. Our proposed CPT-RRT* algorithm augments RRT* as follows: we consider a general continuous cost profile leading to no obstacle collision checking. We also consider both path length and CPT costs with the relative weighting parameter δ for choosing parents and rewiring.

Remark 1: (ER-RRT*). We can obtain the expected risk version of Algorithm 2 by replacing cost function J^c by J^e and following the same procedure as Algorithm 2.

Lemma 1: (Asymptotic Optimality). Assuming compactness of $\mathscr{C}$ and the choice of γ_{RRT^*} according to Theorem 38 in [19], the CPT-RRT* algorithm is asymptotically optimal.

Proof: Please refer to the extended version [28]. ■

VI. CPT-Planner Parameter Adaptation

Here, we aim to compare and evaluate the expressive power of CPT theoretically and experimentally to approximate arbitrary paths in an environment. This method can be used as a first ingredient in a larger scheme aimed at learning the risk perception of a human decision maker,[5] using techniques such as inverse reinforcement learning (IRL). Since our planning problem is defined over a continuous state and action space, CPT can be used for function approximation class in IRL. Then, as is done in IRL, a larger collection of path examples can be used to learn the best weighted combination of specific CPT planners in the class. While certainly of interest, this IRL question is out of the scope of this work. Here we just study the viability of CPT planners as a good function approximation class.

Expressiveness of a risk perception model: Let ρ be a random cost variable and $R(\rho) \in \mathbb{R}_{\geq 0}$ be a risk value function. The expressiveness of two models can be compared by the range of the respective risk value functions.

[5]For offline optimal planning, or in situations where the human does not update the environment online as new information is found.

Definition 1: (Expressiveness). Consider two risk perception models $\mathscr{M}_1$ and $\mathscr{M}_2$ with corresponding classes of risk value functions $\mathscr{V}_1$ and $\mathscr{V}_2$ and respective range spaces $\mathscr{R}_1$ and $\mathscr{R}_2$. We say that $\mathscr{M}_1$ is more expressive ($\geqq$) than $\mathscr{M}_2$ if $\mathscr{R}_2 \subseteq \mathscr{R}_1$ for any given positive random variable ρ. That is, $\mathscr{M}_1 \geqq \mathscr{M}_2 \iff \{R_2(\rho)|R_2 \in \mathscr{V}_2\} \subseteq \{R_1(\rho)|R_1 \in \mathscr{V}_1\}$.

Now, we compare expressiveness of CPT, CVaR[6] and ER.

Lemma 2: Considering ER, CVaR and CPT with corresponding risk value function classes R^e, R^v and R^c defined accordingly, we get: CPT $\geqq$ CVaR $\geqq$ ER.

Proof: First, let us compare ER with CPT and CVaR. The function class R^e has a single function $\mathbb{E}(\rho)$ giving the expected value of ρ, thus the range set of R^e is a singleton, containing $\mathbb{E}(\rho)$. By choosing a function $R^v_0 \in R^v$ and $R^c_{\overline{\Theta}} \in R^c$ with $\overline{\Theta} = \{1, 1, 1, 1\}$, we have $R^v_0(\rho) = R^e(\rho) = R^c_{\overline{\Theta}}$. Which implies $\mathbb{E}(\rho) \in \{R^v_q(\rho)|q \in [0, 1)\}$ and also $\mathbb{E}(\rho) \in \{R^c_\Theta(\rho)|R^c_\Theta \in R^c\}$, thus proving CVar $\geqq$ ER and CPT $\geqq$ ER.

Next let us closely examine CVaR and CPT and then make the concluding comparison. The range space of R^v is $[\mathbb{E}(\rho), b]$, where b is the worst case outcome of ρ. We also know that $\mathbb{E}(\kappa\rho) = \kappa\mathbb{E}(\rho)$. From this we can construct $\kappa_q = \frac{R^v_q(\rho)}{\mathbb{E}(\kappa\rho)}$ which shows that $R^v_q(\rho) = \mathbb{E}(\kappa_q\rho)$. Consider a subclass of CPT value functions $R^c_{\Theta*}$ where $\Theta* \in \{\Theta|\alpha = 1, \beta = 1, \gamma = 1, \lambda = \kappa_q\}$, we have CPT value $R^c_\theta = \mathbb{E}(\kappa_q\rho)$ with $\theta \in \Theta*$. From this, we can say that $\{R^v_q(\rho)|q \in [0, 1)\} \subseteq \{R^c_\theta|\theta \in \Theta*\} \subseteq \mathscr{R}(R^c)$. Putting the two parts together, we get CPT $\geqq$ CVaR $\geqq$ ER, concluding the proof. ■

These arguments imply that risk aversion can equivalently be modeled as an expected value of the scaled random variable, with greater scaling implying higher risk aversion. This is captured in both CPT (λ parameter) and CVaR (q parameter) models. Additionally, CPT also captures risk and uncertainty sensitivity which makes it more expressive than CVaR. Additional empirical visualizations of Lemma 2 can be found in [28]. Next, we will propose a method to evaluate expressiveness in the context of path planning.

Comparing expressiveness in path planning: Let us suppose we have an arbitrary example path P_d drawn in an environment. If the class of CPT planners is expressive enough, we should be able to find a set of parameters that is able to exactly mimic this drawn path. Since an arbitrary path P_d belongs to a very high dimensional space[7] and the planner parameters are typically finite, any amount of tuning may not produce good approximations. We use the term $\mathrm{Ar}(P; P_d) \in \mathbb{R}_{\geq 0}$ to denote the area enclosed between the given path P_d and another path P, thus measuring their closeness. To find the closest path to P_d we have to evaluate

$$\underset{P_\Theta, \Theta \in \mathscr{T}}{\operatorname{argmin}} \mathrm{Ar}(P_\Theta; P_d), \tag{7}$$

where P_Θ is the path produced by CPT-RRT* with CPT parameters Θ, and $\mathscr{T}$ is the set of all possible values of Θ. Directly evaluating (7) is computationally not feasible as the set $\mathscr{T}$ is infinite and resides in $4D$ space.

An alternative to (7) is to use parameter estimation algorithms to determine $\Theta^* \in \mathscr{T}$ which characterizes the path P^* with $\mathrm{Ar}(P_\Theta; P_d)$ as a loss/cost function. We note that neither $\mathrm{Ar}(P_\Theta; P_d)$ can be computed directly, nor the gradient of Ar wrt Θ is accessible. This limits the use of standard gradient descent algorithms to estimate Θ^*. To address this problem, we use SPSA [29] with $\mathrm{Ar}(P_\Theta; P_d)$ as the loss function to estimate the parameters Θ^*. The implementation details of SPSA can be found in [28]. The results are evaluated and compared in Section VII.

VII. Results and Discussion

Here we illustrate the results of the solutions to the problem statement proposed in Sections IV, V, and VI considering a specific scenario having some risk and uncertainty profiles.

Environment Perception and Planning: We consider a scenario where an agent navigates in a room during a fire emergency. The planner is shown a rough floor map (Fig. 3(a)) with obstacles (which are ablaze) in an environment with a blot of ink/torn patch, making that region unclear. This results in a spatial uncertain cost ρ with first moment (ρ_μ) represented by cost associated to obstacles and fire source and second moment (ρ_σ) represented by the uncertainty associated to the ink spot/tear in a $\mathscr{C} = [-10, 10] \times [-10, 10]$ 2D space. The obstacles (blue objects) are ablaze (light orange ellipse) and are known within tolerance (dark green borders). The tear/ink spot (grey ellipse), start (blue dot) and goal (green cross) are also shown on the map. We use a scaled sum of bi-variate Gaussian distribution to model the sources of continuous cost (orange ellipses) with appropriate means and variances to depict the scenario in Fig. 3(a). We utilize bump functions from differential geometry to create smooth "bumps" depicting the discrete obstacles (refer Section III in [28] for more description). Consider the max cost value for the obstacles as $\rho^{\max} \in \mathbb{R}_{\geq 0}$ and let $a_1, a_2, b_1, b_2 \in \mathbb{R}_{\geq 0}$ be the inner (blue rectangle) and outer (dark green borders) measurements of the obstacles from the center $c = (c_1, c_2) \in \mathscr{C}$. Let $x = (x_1, x_2) \in \mathscr{C}$ be a point in the configuration space with f, g, h being real valued scalar functions given by $f(y) = e^{-\frac{1}{y}}, y \in \mathbb{R}_{>0}$ and $f(y) = 0$ otherwise, $g(y) = \frac{f(y)}{f(y)+f(1-y)}$ and $h(y) = 1 - g(\frac{y^2-a^2}{b^2-a^2})$. Then, we calculate $\rho_\mu(x)$ by $\rho_\mu(x) = \rho^{\max} h(x_1 - c_1) h(x_2 - c_2)$.

This is visualized in Fig. 3(b) using $\rho^{\max} = 20$. To generate the second moment of cost ρ_σ, we use a scaled bi-variate Gaussian distribution with appropriate means and variances to depict the ink spot/tear in Fig. 3(a). Now we will illustrate the results of implementing Algorithm 2 in this environment.

CPT-RRT Simulations:* We use a discretization factor $M = 20$ to generate the costs $\rho(x)$ and their corresponding $p(x)$ from Section IV. The results of using Algorithm 1 to every point in $\mathscr{C}$ is shown in Fig. 3, risk R^c or R^e is indicated by color map. Fig. 1(a) shows a rationally perceived environment using expected risk R^e. Whereas, Fig. 1(b) indicates a non-rational highly risk averse perception using CPT (R^c) with $\Theta = \{0.74, 2, 0.9, 10\}$ having a high λ value. Risk indifferent profile (Fig. 3(d)) is generated by $\Theta = \{0.74, 1, 0.3, 2.25\}$ having a low risk sensitivity γ value.

[6]CVaR uses a single parameter $q \in [0, 1]$ representing the fraction of worst case outcomes to evaluate expected risk of an uncertain cost ρ. We will use R^v_Q to denote the perceived risk by CVaR model with $q = Q$. So a $q \approx 1$ considers the worst case outcome of ρ and a $q = 0$ considers all the outcomes thus making $R^v_0 = R_E$.

[7]A path can be modeled as a curve defined by possibly infinite parameters.

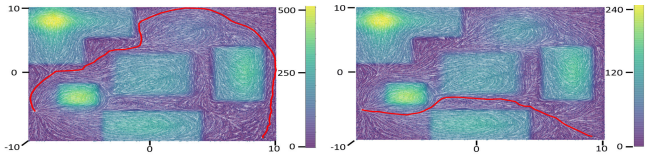

(a) High cost aversion and uncertainty sensitivity ($\Theta = \{0.74, 1, 0.9, 10\}$)

(b) Medium cost aversion and high uncertainty sensitivity ($\Theta = \{0.74, 1, 0.9, 5\}$)

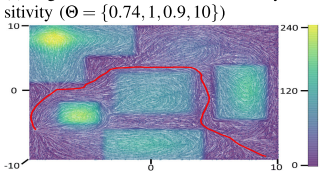

(c) Medium cost aversion and low uncertainty sensitivity ($\Theta = \{0.74, 2, 0.9, 5\}$)

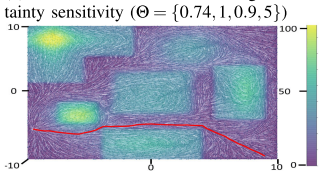

(d) Expected Risk

Fig. 4. Paths produced by CPT-RRT* under different perception models. White lines indicate the tree grown from the start position, red line indicates the optimal path to goal after $T = 20\,000$ iterations. Background color map depicts the CPT costs in (a)-(c) and expected costs in (d)

Similarly, uncertainty indifferent profile (Fig. 3(e)) and uncertainty averse profile (Fig. 3(f)) are generated by fixing α and having high and low β values respectively. Next, Algorithm 2 is used to plan a path from the start point to the goal point shown in Fig. 3(a). We use $T = 20\,000$ iterations for the CPT-RRT* algorithm with $\delta = 10^{-4}$. The same random seed was used for consistency. The path planning results are illustrated in Fig. 4. Fig. 4(a) indicates a circuitous path due to the highly risk averse perception, whereas Fig. 4(d) indicates a shorter and more direct path for a rational DM using expected risk. Increasing the uncertainty sensitivity (lowering β) and reducing risk aversion (lowering λ) makes the planner avoid the highly uncertain ink spot/tear in the top-right region and take a more riskier path in the lower region as shown in Fig. 4(b). By having a medium risk aversion and lower uncertainty sensitivity (increasing β), the planner produces a different path as shown in Fig. 4(c).

Solution quality: Fig. 5(a) and Fig. 5(b) illustrates the empirical convergence and solution quality of the paths produced. For empirical convergence, we ran CPT-RRT* 100 times with the same parameters and initial conditions while measuring the distance between paths produced every 500 iterations, for 80 000 iterations. The results are shown in Fig. 5(a). We see that initially ($< 10\,000$ iterations) there are changes in the output path as the space is being explored. After 10 000 iterations we consistently see minimal path changes indicating that the algorithm is converging. Then we checked the solution quality by computing the cost of the output path every 250 iterations as shown in Fig. 5(b) for 100 trials consisting of 25 000 iteration. We see that the there is a consistent decrease in path cost and after 10 000 iterations it starts to plateau, indicating that the algorithm is close to a high quality (low cost) solution. We recommend $T \geq 10\,000$ to achieve smooth and consistent paths in our setting.

Comparison in narrow and cluttered environments: Here, we will illustrate and compare our RRT* framework with T-RRT* [24] in a cluttered environment (100 random objects in right half) with a long narrow passage (left half) as shown in Fig 5. The start point x_s is on the top right corner and the goal x_g is at the center of narrow passage. Bump functions similar to previous paragraphs were used to construct a smooth spatial cost ρ from obstacles. Since T-RRT* does not have risk/uncertainty perception capabilities, we use the continuous cost ρ for both algorithms. This allows us to specifically compare the algorithms' planning capabilities in the same continuous cost environment. We used $\gamma_{\text{RRT}^*} = 100$ and $d = 0.35$ in both cases. From Fig. 5(c) we can see that our algorithm is able to sample and generate paths in the narrow passage, as well as to avoid obstacles in a cluttered environment. In comparison, we can see that T-RRT* employing integral cost (IC) in Fig. 5(d) and minimum work (MW) in Fig. 5(e) cannot generate paths in the narrow costly region fast enough irrespective of the T_{Rate} used. Also, T-RRT* paths do not appear to be as smooth as the paths from our framework, irrespective of the cost (IC or MW) used. We believe that the reason for the above observations is that cluttered and high cost environments induce a high failure rate of the transition test, resulting in a sampling bias and longer run times for T-RRT* to build the same number of nodes as our algorithm, especially for high T_{Rate} values.

Additional results showing change in paths due from varying δ and illustration of CPT-RRT* in a 3D environment are presented in [28] due to space constraints. Overall, our planner's risk-perception-aware paths are logically consistent in a given risky scenario.

Comparison in dynamic environments: Here, we contrast the performance of CPT-RRT* and Risk-RRT* [21] (a risk aware planner) in a 10 by 10 environment area with static and moving obstacles as shown in Fig. 6. To account for risk dynamics, we will be planning in the space-time domain, and assume knowledge of the dynamics (or a good estimate) of $\rho_\mu(t)$ and $\rho_\sigma(t)$, which will result in a time-varying perceived risk map $R^c(x,t)$. We also assume that each edge in the tree will be traversed in some time Δt. The underlying RRT* parameters employed by both algorithms were taken to be identical, with $\gamma_{RRT*} = 100$ and $d = 0.25$, while $\delta = 0.1$ for CPT-RRT*. Our starting point is the same parametric CCR Risk Map [30] as in Risk-RRT*, which generates a continuous, and time-varying, cost map based on the pose and velocity of a moving human as shown in Fig. 6(a) (a snapshot). The human obstacles move back and forth within the indicated range (gray line), with top two obstacles moving d units in Δt time, while middle left obstacle moves at $0.1d$ units. Since the CCR map does not incorporate uncertainty, we will use it as the mean cost $\rho_\mu(t)$. We employ a scaled normal distribution on top of each source of dynamic risk (moving human) to denote $\rho_\sigma(t)$, representing uncertainty for each source. From $\rho_\mu(t)$ and $\rho_\sigma(t)$, we calculate $R^c(x,t)$ according to Algorithm 1 which is visualized in Fig. 6(c). Note that with higher risk (moving obstacles as compared to static or no obstacles), the lighter the color in the map. We compare our algorithm with Risk-RRT* in two scenarios. At first, for fair comparison, and since Risk-RRT* does not consider uncertainty or risk perception models, we use directly the CCR cost map or $\rho_\mu(t)$ for planning. This corresponds to a rational DM model. The results are summarized in Fig. 6(b) which show path length and cumulative risk returned by CPT-RRT* and Risk-RRT* using the CCR map in 50 trials. We use a risk threshold of 0.1 to implement Risk-RRT*. In general, we see a lower performance in Risk-RRT* due to its conservative approach in dealing with risk. First, since risk is not explicitly accounted for in the cost

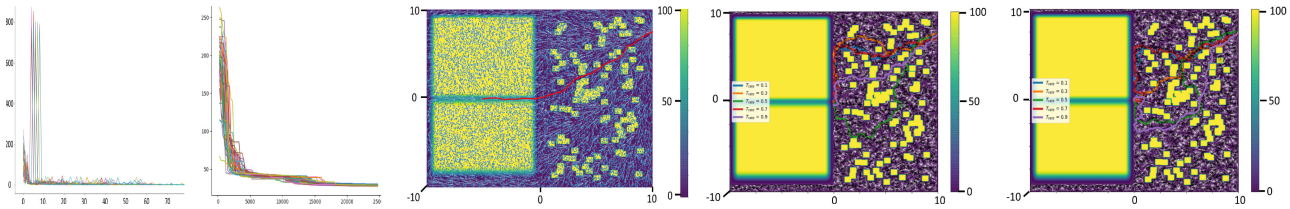

(a) Convergence over iterations (b) Path cost over iterations (c) Paths produced by CPT-RRT*. (d) Paths produced by T-RRT* using IC. (e) Paths produced by T-RRT* using MW.

Fig. 5. Solution quality and T-RRT* path comparison. a) Distance between paths every 500 iterations (y-axis) and number of iterations in 1000 (x-axis). b) Cost of output path (y-axis) every 250 iterations with number of iterations (x-axis) (c)-(e) Paths produced in a cluttered environment using $T = 20\,000$ iterations for CPT-RRT* and 20 000 nodes for T-RRT*.

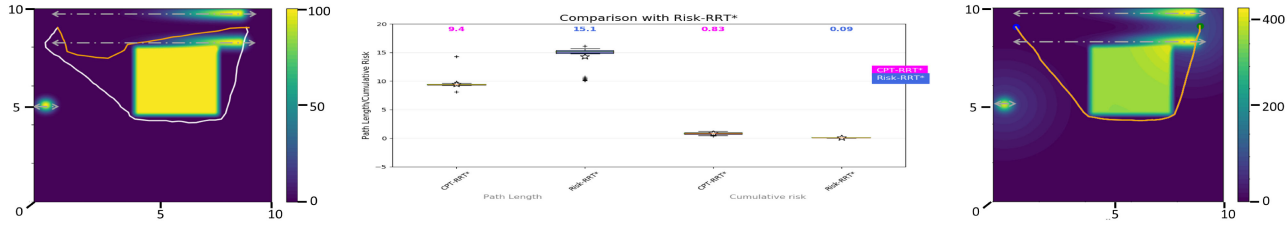

(a) Paths returned by CPT-RRT*(Orange) and Risk-RRT*(White) in CCR map (b) Boxplots showing path length and cumulative risk returned by CPT-RRT* and Risk-RRT* using the CCR map in 50 trials (38 trials for Risk-RRT* as 12 did not succeed in finding a path) consisting of 15,000 RRT* iterations. (c) Paths returned by CPT-RRT*(Orange) in risk averse perception of CCR map with $\Theta = \{0.74, 1, 0.88, 6.25\}$

Fig. 6. Comparison with Risk-RRT*. The CCR Map containing 3 moving humans and a stationary obstacles at initial time is shown in the background.

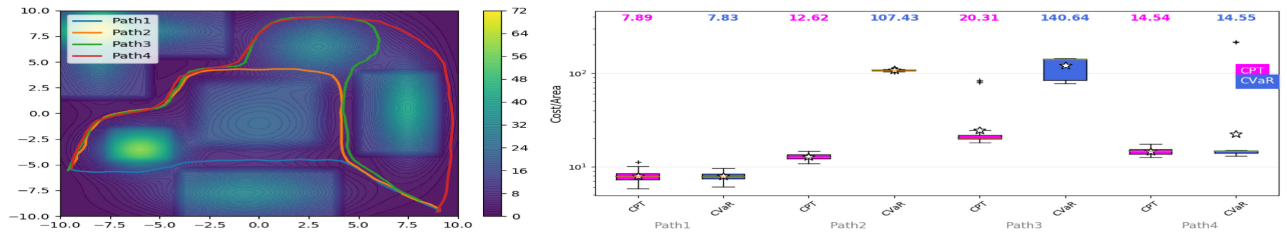

(a) Four paths $\{P_d^1, P_d^2, P_d^3, P_d^4\}$ are drawn in blue, orange, green and red respectively. (b) Boxplots showing the cost(Area) returned after using SPSA with CPT and CVaR to capture risk profile of the drawn paths.

Fig. 7. Result of using CPT and CVaR to model drawn paths.

function of Risk-RRT* and "risk" is treated as an "obstacle" to avoid, the resulting path produced by Risk-RRT* is longer, even though its cost function optimizes path length. The length of the path from our planner is shorter, with comparable cumulative risk of the output paths of both planners computed as in (6). Furthermore, 12 out of the 50 trials in case of Risk-RRT* could not find a solution within 15 000 iterations. This seems to be a consequence of a higher sample rejection rate due to the tight free spaces created by the dynamic obstacles when close to other objects. This drawback is more pronounced when considering a risk-averse DM. Fig. 6(c) represents such DM who perceives that getting close to the dynamic obstacles is highly risky, as compared to the perception of a rational DM represented by Fig. 6(a). In this way, the risk values in Fig. 6(c) are in the range $0 - 421$, which is much higher than those of the CCR Map in Fig. 6(a) (with ranges $0 - 100$). Due to higher risk values as given by this map, the sample rejection in Risk-RRT* is very high and could not find a feasible path in any of 50 trials, whereas CPT-RRT* consistently found a path similar to the one shown in Fig. 6(c) in all of the 50 trials.

CPT planner expressive power evaluation: We now discuss the proposed framework in Section VI to gauge the expressiveness of CPT as a perception model to depict a drawn path P_d. To implement SPSA, we follow guidelines from [29]. The exact parameter choice is detailed in [28]. We choose the nominal parameters $\Theta_0 = \{0.74, 1, 0.88, 2.25\}$ from [4] for CPT throughout the simulation, and $q_0 = 0.5$ for the CVaR variant. We use the same environment as in Fig. 3 for all the simulations. Four different paths $\{P_d^1, P_d^2, P_d^3, P_d^4\}$ are drawn by hand on the expected risk profile (Fig. 4(d)) shown in Fig. 7(a). Path P_d^1 is similar to a path generated with expected risk perception (Fig. 4(d)). Whereas, path P_d^4 and P_d^2 are similar to paths generated with high risk aversion (Fig. 4(a)) and uncertainty insensitivity (Fig. 4(c)) respectively. Path P_d^3 is more challenging to represent as it shows an initial aversion to risk and uncertainty and then takes a seemingly costlier turn at the top. We then use our proposed SPSA approach with a tolerance $\kappa = 15$ and a maximum of 10 SPSA iterations per trial. We use $T_k = 15\,000$ and $\delta = 0.01$ to implement Algorithm 2 to determine the loss Ar during each SPSA iteration. For CVaR,

the planner (Algorithm 2) replaces R^c with R^v in order to use perceived risk according to CVaR while the rest of the planner framework remains unchanged. At the end each trial we get the loss Ar between the returned P_Θ and the drawn path P_d^x.

We represent the statistics of the returned cost Ar as boxplots as shown in Fig. 7(b). Each box plot represents the distribution of 50 returned Ar values after each trial for each path and perception model. The Y-Axis represents Ar in a base 10 log scale. We calculate a few sample areas: $\mathrm{Ar}(P_d^1, P_d^2) = 99.14, \mathrm{Ar}(P_d^2, P_d^3) = 35.20$ and $\mathrm{Ar}(P_d^3, P_d^4) = 73.41$ to give a quantitative idea of the measure Ar in this scenario to the reader. The median values for each box plot is indicated on the top row. The mean value of the distribution is indicated as "stars," the black lines above and below the box represent the range, and $+$ indicates outliers. We observe that from Fig. 7(b), both Path P_d^1 and Path P_d^4 were captured equally well with CVar and CPT with low Ar values. Since both CPT and CVaR are generalizations of expected risk, paths close (like P_d^1) to paths generated from expected risk can be easily mimicked. Similarly, since CPT and CVaR are designed to capture risk aversion, paths close (like P_d^4) to risk averse paths (Fig. 4(a)) can also be easily captured. However, we see a contrast in performance for path P_d^2 and path P_d^3. CPT, on both occasions, is able to track the drawn paths reasonably well with low Ar values. Whereas CVaR has consistently higher (an order of magnitude) Ar values, indicating the inability to capture the risk perception leading to path P_d^2 and path P_d^3. This is due to the fact that CPT can handle uncertainty perception independently from the cost (Fig. 3(e) and Fig. 3(f)). This ability is needed to capture paths like P_d^2 and P_d^3 which is lacking in models like CVaR and expected risk. This result confirms the theoretical arguments of Lemma 2 and shows richer modeling capability of CPT.

VIII. Conclusions and Future Work

We have proposed a novel adaptation of CPT to model a DM's non-rational perception of a risky environment in the context of path planning. Firstly, using CPT, we provide a tuning knob to model various risk perceptions of an uncertain spatial cost. Next, we demonstrate a novel embedding of non-rational risk perception into a sampling based planner, the CPT-RRT*, to plan asymptotically optimal paths in perceived environments. Finally, we theoretically and empirically evaluate CPT as a good approximator to the risk perception of arbitrary drawn paths by comparing against CVaR, and show that CPT is a richer model approximator. Future work will analyze how CPT can be used to learn the risk profile of a DM using learning frameworks and conducting user studies.

References

[1] H. Choset *et al.*, *Principles of Robot Motion: Theory, Algorithms and Implementations*. Cambridge, MA, USA: The MIT Press, 2005.

[2] C. Wu, A. Bayen, and A. Mehta, "Stabilizing traffic with autonomous vehicles," in *Proc. IEEE Int. Conf. Robot. Automat.*, 2018, pp. 1–7.

[3] A. Suresh and S. Martínez, "Human-swarm interactions for formation control using interpreters," *Int. J. Control, Automat. Syst.*, vol. 18, pp. 2131–2144, 2020.

[4] A. Tversky and D. Kahneman, "Advances in prospect theory: Cumulative representation of uncertainty," *J. Risk Uncertainty*, vol. 5, no. 4, pp. 297–323, 1992.

[5] H. Kurniawati, T. Bandyopadhyay, and N. M. Patrikalakis, "Global motion planning under uncertain motion, sensing, and environment map," *Auton. Robots*, vol. 33, no. 3, pp. 1–18, 2012.

[6] J. Song, S. Gupta, and T. Wettergren, "T*: Time-optimal risk-aware motion planning for curvature-constrained vehicles," *IEEE Robot. Automat. letters*, vol. 4, no. 1, pp. 33–40, Jan. 2019.

[7] B. Burns and O. Brock, "Sampling-based motion planning with sensing uncertainty," in *Proc. IEEE Int. Conf. Robot. Automat.*, 2007, pp. 3313–3318.

[8] B. Luders, S. Karaman, and J. How, "Robust sampling-based motion planning with asymptotic optimality guarantees," in *Proc. AIAA Conf. Guid., Navigation Control*, Aug. 2013, pp. 1–27,.

[9] L. Blackmore, M. Ono, and B. C. Williams, "Chance-constrained optimal path planning with obstacles," *IEEE Trans. Robot.*, vol. 27, no. 6, pp. 1080–1094, Dec. 2011.

[10] N. E. D. Toit and J. W. Burdick, "Robot motion planning in dynamic, uncertain environments," *IEEE Trans. Robot.*, vol. 28, no. 1, pp. 101–115, Feb. 2012.

[11] S. Singh, Y. Chow, A. Majumdar, and M. Pavone, "A framework for time-consistent, risk-sensitive model predictive control: Theory and algorithms," *IEEE Trans. Autom. Control*, vol. 64, no. 7, pp. 2905–2912, Jul. 2019.

[12] A. Hakobyan, G. Kim, and I. Yang, "Risk-aware motion planning and control using CVaR-constrained optimization," *IEEE Robot. Automat. Lett.*, vol. 4, no. 4, pp. 3924–3931, Oct. 2019.

[13] P. Artzner, F. Delbaen, J. Eber, and D. Heath, "Coherent measures of risk," *Math. Finance*, vol. 9, no. 3, pp. 203–228, 1999.

[14] S. S. Stevens, "On the psychophysical law," *Psychol. Rev.*, vol. 64, no. 3, pp. 153–181, 1957.

[15] S. Gao, E. Frejinger, and M. Ben-Akiva, "Adaptive route choices in risky traffic networks: A prospect theory approach," *Transp. Res. Part C: Emerg. Technol.*, vol. 18, no. 5, pp. 727–740, 2010.

[16] A. R. Hota and S. Sundaram, "Game-theoretic protection against networked sis epidemics by human decision-makers," *IFAC Papers Online*, vol. 51, no. 34, pp. 145–150, 2019.

[17] C. Jie, P. L. A., M. Fu, S. Marcus, and C. Szepesvari, "Stochastic optimization in a cumulative prospect theory framework," *IEEE Trans. Autom. Control*, vol. 63, no. 9, pp. 2867–2882, Sep. 2018.

[18] L. Wang, Q. Liu, and T. Yin, "Decision-making of investment in navigation safety improving schemes with application of cumulative prospect theory," *J. Risk Rel.*, vol. 232, no. 6, pp. 710–724, 2018.

[19] S. Karaman and E. Frazzoli, "Sampling-based algorithms for optimal motion planning," *Int. J. Robot. Res.*, vol. 30, no. 7, pp. 846–894, 2011.

[20] B. Boardman, T. Harden, and S. Martínez, "Limited range spatial load balancing in non-convex environments using sampling-based motion planners," *Auton. Robots*, vol. 42, no. 8, pp. 1731–1748, 2018.

[21] W. Chi and M. Q. Meng, "Risk-RRT*: A robot motion planning algorithm for the human robot coexisting environment," in *Proc. Int. Conf. Adv. Robot.*, 2017, pp. 583–588.

[22] B. Englot, T. Shan, S. D. Bopardikar, and A. Speranzon, "Sampling-based min-max uncertainty path planning," in *Proc. IEEE Int. Conf. Decis. Control*, 2016, pp. 6863–6870.

[23] E. Schmerling, K. Leung, W. Vollprecht, and M. Pavone, "Multimodal probabilistic model-based planning for human-robot interaction," in *Proc. IEEE Int. Conf. Robot. Automat.*, 2018, pp. 1–9.

[24] D. Devaurs, T. Simeon, and J. Cortes, "Optimal path planning in complex cost spaces with sampling-based algorithms," *IEEE Trans. Automat. Sci. Eng.*, vol. 13, no. 2, pp. 415–424, Apr. 2016.

[25] T. Shan and B. Englot, "Sampling-based minimum risk path planning in multiobjective configuration spaces," in *Proc. IEEE Int. Conf. Decis. Control*, 2015, pp. 814–821.

[26] S. Dhami, *The Foundations of Behavioral Economic Analysis*. London, U.K.: Oxford Univ. Press, 2016.

[27] D. Prelec, "The probability weighing function," *Econometrica*, vol. 66, no. 3, pp. 497–527, 1998.

[28] A. Suresh and S. Martínez, "Planning under non-rational perception of uncertain spatial costs," 2020, *arXiv:1904.02851*.

[29] J. C. Spall, *Introduction to Stochastic Search and Optimization*. New York, NY, USA: Wiley, 2003.

[30] W. Chi, H. Kono, Y. Tamura, A. Yamashita, H. Asama, and M. Q. Meng, "A human-friendly robot navigation algorithm using the risk-rrt approach," in *Proc. IEEE Int. Conf. Real-time Comput. Robot.*, 2016, pp. 227–232.